JOURNAL OF APPLIED ELECTROCHEMISTRY 22 (1992) 57–63

Influence of surface segregation of sulphur on the corrosion resistance of 270 nickel in acidic and alkaline media

P. RABU

IPCM, 2 rue de la Houssinière, 44072 Nantes, Cédex 03, France

G. SAINDRENAN

ISITEM, La Chantrerie, 44087 Nantes, Cédex 03, France

A. CAPRANI

INSERM U256, 96 rue Didot, 75674 Paris, Cédex 14, France

T. JASZAY, J. P. FRAYRET

ENSM, Laboratoire d'Energétique, 1 rue de la Noë, 44072 Nantes, Cédex 03, France

Received 24 April 1990; revised 7 May 1991

270 Nickel has a sulphur content lower than 1 p.p.m. However, surface concentrations close to saturation values can be obtained after several hours of cold-hammering followed by annealing procedures. The effects of this segregation on the electrochemical behaviour of nickel are analysed using current–potential curves and by examining the corrosion features via scanning electron microscopy (SEM). An overall increase in dissolution for the nickel with surface segregation of sulphur with respect to the homogeneous metal is observed in acidic (1 M H_2SO_4) as well as in alkaline medium [(K_2SO_4 + LiOH) at pH 9.5]. The reaction model proposed here, which depicts the dissolution kinetics, allows specification of the depassivating role of sulphur.

1. Introduction

Nickel is frequently involved in the composition of numerous alloys, either as a basic (Inconel, Hastelloy) or an additional element (steels). Due to its surface properties, nickel also acts as a catalyst in certain reactions. It has long been observed that these properties are affected by the presence of sulphur (poisoning of catalysts [1], fragility during cold or warm forming [2]). Surface sulphur may arise from the environment, through adsorption, or from the material itself, through a mechanism of segregation [3]. In the latter case, segregation is established according to the thermodynamic and kinetic laws of equilibrium segregation. Equilibrium segregation generally occurs when the conditions of use lead to, or require, annealing procedures at temperatures such as $\theta_r \approx 0.5\,\theta_F$ (θ_r = annealing temperature and θ_F = melting temperature) [1]. Provided that the kinetics are fast enough, segregation decreases when temperature increases.

However, it is also possible to generate surface segregation starting from nickel out of thermodynamic equilibrium [4], for example, from cold-hammered nickel, by recovering equilibrium conditions through recrystallization annealing. This recovering procedure is characterised by germination and growth of new grains which form at the cost of the cold-hammered matrix. In that case, impurities, in particular sulphur, can stabilize at the grain boundaries and onto the surface [5]. The main feature of this process is its rapidity with respect to the equilibrium mechanism. Since segregation decreases by increasing the recrystallization temperature and since this temperature is lowered by increasing the metal purity, then the segregation extent will be the higher when the metal is pure. Therefore, interface segregations are induced at temperatures where the slowness of the kinetics blocks the equilibrium mechanism.

These two modes of obtaining segregation, *i.e.* from nickel in and out of thermodynamic equilibrium, have similar effects [6]. More especially, the electrochemical behaviour of nickel is markedly affected by sulphur segregation. In fact, a highly accelerating effect of sulphur on nickel dissolution in acidic medium was shown by Marcus [7], in the case of a nickel monocrystal covered with a layer of adsorbed sulphur. This effect was interpreted in terms of a delay in the formation of the passive layer, which attenuates its protective properties.

The present investigation considers the influence of sulphur segregation, as obtained through the out-of-equilibrium process on nickel resistance to corrosion, using electrochemical methods and scanning electron microscopy.

0021-891X/92 $03.00 + .12

Table 1. Chemical composition of 270 Ni (analysis by spark emission spectrometry using an ARL device)

Element	*Fe*	*Mn*	*O*	*C*	*S*	$\sum$ *others*
Weight (p.p.m.)	30	20	70	21	0.5	50

2. Materials and methods

2.1. *Materials*

Samples were taken from a 270 nickel rod (Ni $\geqslant$ 99.99%; see Table 1). The carbon content (20 p.p.m.) was indicative of the ex-carbonyl origin of the alloy. Plastic deformations were obtained by cold uniaxial traction of a nickel rod previously annealed in the basal state (Table 2). All the annealing processes were performed under vacuum in a sealed silicon container. This treatment may, of course, induce desorption of impurities which can in turn concentrate at the material surface. A thermal treatment in neutral gas atmosphere under pressure would have been more appropriate; however, we adopted a vacuum procedure because no adequate oven was available to us. The sample was taken from a traction test-piece which was cold hammered at a given value, ε, of the deformation ratio. After this preparation, the sample surface (initially polished with an abrasive paper up to grade 600) was no longer subjected to any mechanical or chemical process liable to alter it. Table 2 reports the various types of samples investigated.

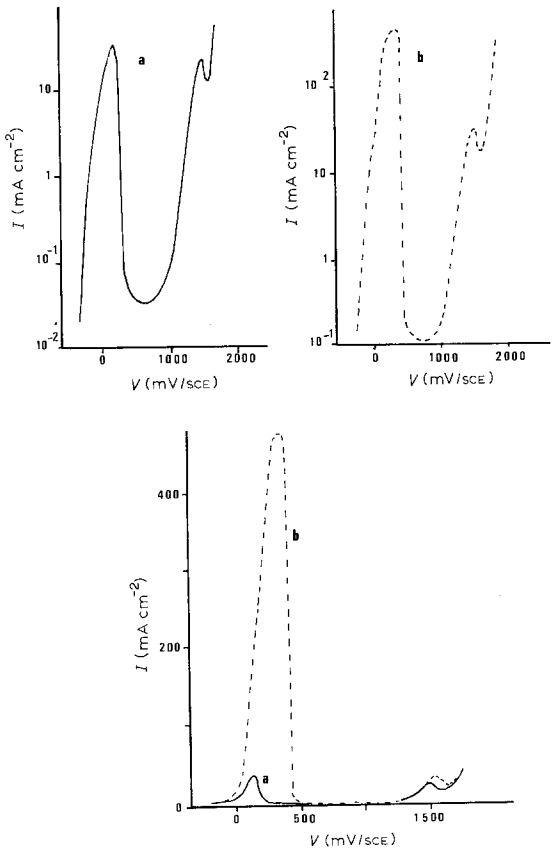

Fig. 1. Potentiodynamic *I–V* curves. U argon-deaerated 1 M H_2SO_4 at 23.5° C; nickel (diam. 5 mm) — no rotation; polarization (sweep) rate 6 mV min^{-1}. (a) 270 Ni (reference) and (b) 270 Ni (recrystallized).

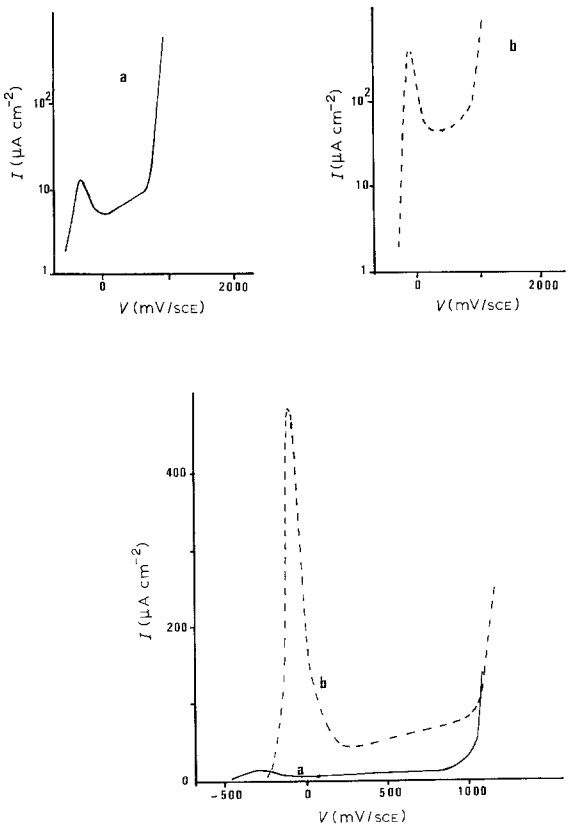

Fig. 2. Potentiodynamic *I–V* curves. U argon-deaerated 0.1 M K_2SO_4 + 10^{-4} M LiOH; pH ~9.5; at 23.5° C; nickel (diam. 5 mm) — no rotation; polarization (sweep) rate 6 mV min^{-1}. (a) 270 Ni (reference) and (b) 270 Ni (recrystallized).

2.2. *Electrolytes*

Most studies concerning the influence of sulphur on the electrochemical behaviour of nickel have been carried out in the presence of sulphuric acid [7]. The present study dealt with sulphuric acid as well as alkaline medium. 1 M sulphuric acid was obtained from a Merck concentrated product and bidistilled water. The alkaline medium was a K_2SO_4 + LiOH aqueous solution at pH ~9.5.

The alkaline medium was chosen because of its importance in the nuclear industry and the scarcity of literature on media at pH's close to or higher than 7; although such instances in the latter case have numerous industrial applications either in the case of nickel or its alloys. Nickel-made materials are highly important in the nuclear industry. We therefore deemed it of interest to investigate the influence of a medium similar to cooling waters for nuclear reactors, which flow through steam generators. These waters are strongly deionized and kept at pH 9.5 with a low LiOH concentration (~10^{-4} M). This medium is poorly conductive and does not permit accurate electrochemical measurements. Hence, we added a supporting electrolyte such as 0.1 M K_2SO_4 which plays no role in the reactions at the interface investigated. Moreover, this choice allows comparison with the

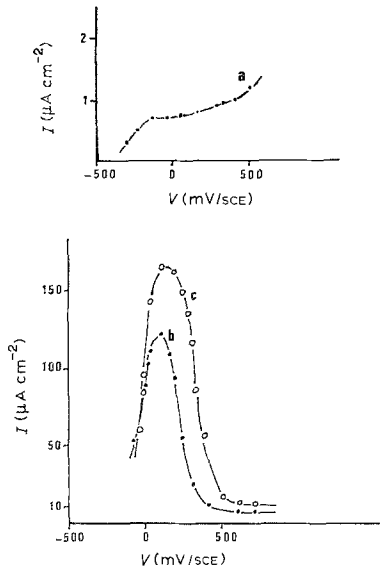

Fig. 3. Steady-state I–V curves. U argon-deaerated 0.1 M K_2SO_4 + 10^{-4} M LiOH, pH ~9.5 at 23.5° C. Nickel (diam. 5 mm) – rotation speed 1000 r.p.m.; polarization (sweep) rate 6 mV min^{-1}. (a) 270 Ni (reference), (b) 270 Ni (recrystallized no. 2); $\varepsilon = 0.1$ and (c) 270 Ni (recrystallized no. 2); $\varepsilon = 0.25$.

acidic medium since the main difference between these media lies merely in pH and sulphate ion concentration.

2.3. *Experimental techniques*

Current–potential curves were obtained using a standard three-electrode potentiostatic device (Tacussel PRT 20-2X potentiostat). The working electrode (investigated metal) was a 5 mm diameter disc, which was the cross-section of a 270 nickel rod. The lateral side of the rod was covered either with varnish or a thermoretractable polyolefin sheath, according to the test conditions. The surface of the disc was polished with abrasive paper up to grade 600. Mechanical polishing, instead of chemical or electrochemical, was chosen in order to avoid contamination of the sample surface by the bath constituents and to prevent the insulating sheath from being unstuck. In addition, mechanical polishing plays no role in corrosion morphology, as shown by SEM (see Fig. 4), since the polishing grooves, still present after the corrosion process, do not modify the distribution of the preferential attack sites. The reference electrode was a double-junction saturated-KCl calomel electrode (SCE). The counter-electrode was a large area platinum grid. The cell was maintained at 23.5° C by water circulation. The disc electrode was rotated using a set-up described elsewhere [8]. Deaeration of the medium was obtained by argon bubbling.

The effect of sulphur segregation is so important that steady-state polarization plots cannot be obtained in the acidic medium. Therefore, such curves were plotted in less acidic media, mainly in order to show up a possible influence of mass transfer by convective diffusion.

Corrosion morphology was examined by SEM (JEOL JSM 35C).

3. Experimental results

3.1. *Current-potential curves*

3.1.1. Dynamic polarization. After a 2 h immersion of the sample (time required to stabilize the rest potential), I–V curves were recorded at increasing potentials. Figures 1 and 2, for a sweep rate of 6 mV min^{-1}, represent the I–V curves for the 1 M H_2SO_4 and the 0.1 M K_2SO_4 + 10^{-4} M LiOH media, respectively. For each medium, the curves for the reference nickel and the recrystallized nickel with sulphur segregation are plotted (curves a and b). A comparison of curves a and b, when plotted using the same scale, shows the important role of the thermomechanical process. Table 3 provides the values of the typical quantities. It may be noted that the presence of sulphur at the surface of both types of recrystallized nickel leads to an increase in the peak and passive currents and to a shift of the rest and peak potentials towards anodic values quite independently of pH value.

3.1.2. Steady-state polarization. As mentioned above, steady-state polarization plots can be obtained with the K_2SO_4 + LiOH medium only. No significant contribution of convective diffusion was observed at rotation speeds ranging from 0 to 5000 r.p.m. Therefore, all the curves were plotted at 1000 r.p.m. The curves for the reference metal and those for that having undergone a deformation are shown in Fig. 3. The trends observed under potentiodynamic conditions are still maintained. However, a lower amplitude inherent in the polarization mode is noted. This discrepancy shows that the potential sweep rate chosen leads only to a pseudo steady-state.

3.2. *Corrosion morphology*

The morphology of the corroded surfaces was observed subsequently to the potentiodynamic curves.

Table 2. Thermomechanical properties of the test samples and techniques.

Material 270 Ni	*Cold-hammering ratio ε*	*Annealing under vacuum*	*Potentiostatic or time-dependent study*
Reference state	0	100° C – 5 h	Potentiostatic and time-dependent
Recrystallized no. 1	0.15	500° C – 63 h	Time-dependent
Recrystallized no. 2	0.1 and 0.25	600° C – 48 h	Potentiostatic

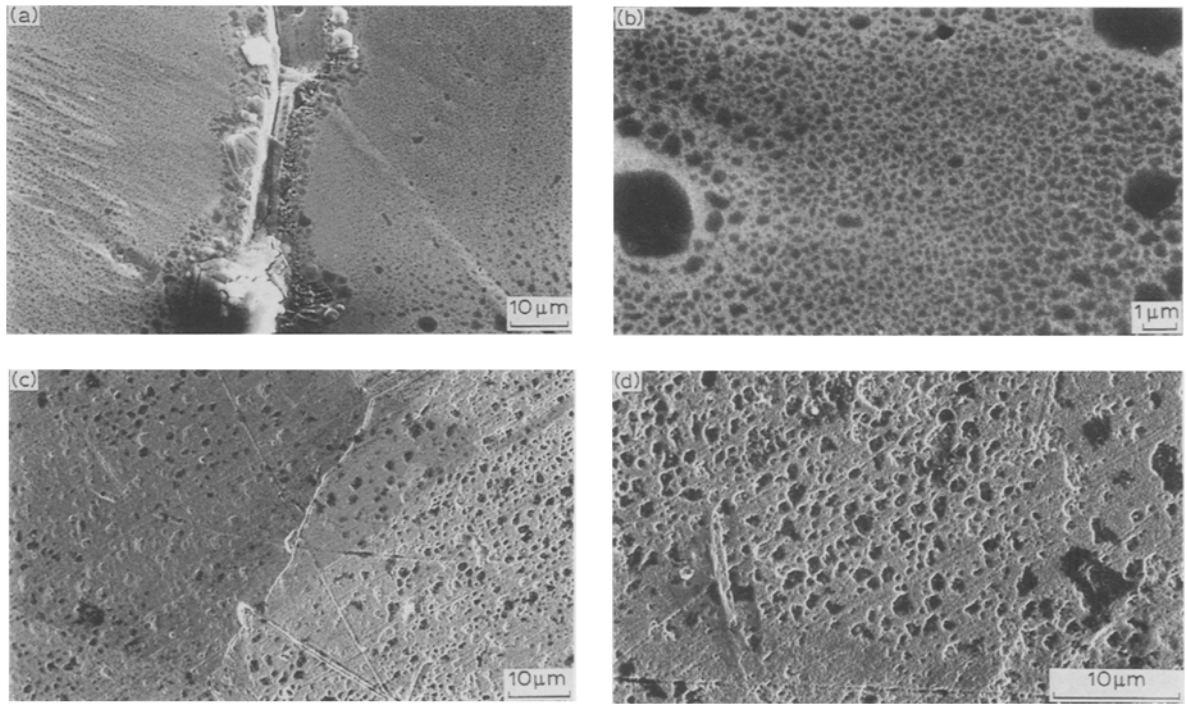

Fig. 4. SEMs showing the corrosion states in 1 M H_2SO_4 (a and b) and in (K_2SO_4 + LiOH) (c and d)

Examination of the micrographs of Fig. 4 leads to three conclusions:

(i) the grain boundaries are attacked in both media, but strongly in the acidic and only slightly in the K_2SO_4 + LiOH medium;

(ii) corrosion in the K_2SO_4 + LiOH medium leads to a less marked surface roughness; and

(iii) the grain surface exhibits big holes randomly distributed in both media. In addition, in the alkaline medium two scales of holes are present.

4. Discussion

Steady-state polarization curves (which can be obtained in the alkaline medium only) show that the reference nickel remains inert over the whole range of potential investigated. In contrast, the samples which have undergone a thermomechanical process display a passive-like behaviour (bell-shaped I–V curves).

Considering previous models proposed in the literature under different conditions [9, 10], the bell-shape of the I–V curves, and the oxidation states of nickel in the dissolution intermediates (+1 and +2), a further model involving a bifurcation at the level of Ni(+1) intermediate adsorbate may be proposed. The simplest model, with respect to the number of steps, entails three electrochemical reactions and one chemical reaction, as shown in Fig. 5. This model allows competition between two reaction branches that both lead to divalent nickel in solution. The reaction branch that implies the adsorbed intermediate Ni(II) leads to passivation. Ni(II) most probably corresponds to a hydroxide $Ni(OH)_2$ or to an oxide (NiO) when passivity is stable.

As indicated previously for titanium [11–14], it is assumed that adsorption obeys the Langmuir isotherm and that the system is in steady-state. Thus, this model leads to the following I–V relationship:

$$I = \frac{2F(K_2 + K_3)}{1 + \frac{K_2}{K_1} + K_3\left(\frac{1}{K_1} + \frac{1}{K_4}\right)} \qquad (1)$$

where $K_1 = K_1^0 e^{aV}$, $K_2 = K_2^0 e^{b_1 V}$, $K_3 = K_3^0 e^{b_2 V}$, i.e. the rate of the electrochemical steps which lead to valences I and II obey Tafel's law (a, b_1, b_2 are the Tafel exponents). K_4 is the rate of the chemical step for the passage into solution of divalent nickel starting

Table 3. Characteristic currents and potentials

Medium	*Sample*	*Rest potential (mV/SCE)*	*Peak current ($\mu A\,cm^{-2}$)*	*Peak potential (mV/SCE)*	*Primary passivity current at 600 mV/SCE ($\mu A\,cm^{-2}$)*
H_2SO_4	Ni reference	−324	38 000	125	34
H_2SO_4	Ni recrystallized no. 2	−300	447 000	330	125
K_2SO_4 + LiOH	Ni reference	−550	13.3	−320	6.3
K_2SO_4 + LiOH	Ni recrystallized no. 2	−421	486	−180	4.7

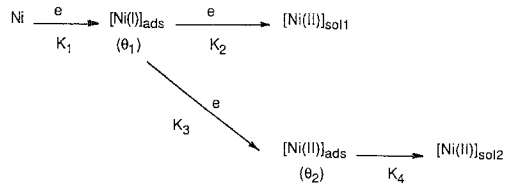

Fig. 5. Model for the dissolution–passivation of Ni in neutral and alkaline media (seven kinetic parameters).

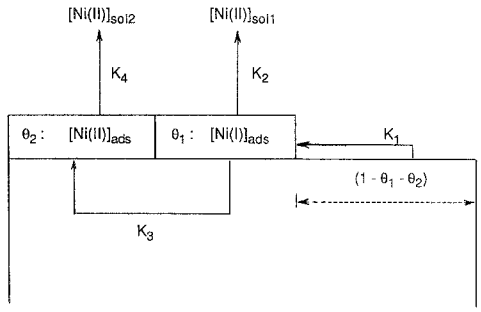

Fig. 6. Schematic representation of interface phenomena between the metal substrate and the electrolyte for a unit surface: θ_1 and θ_2 represent the coverage fractions of the reaction intermediates.

from the adsorbate $[Ni(II)]_{ads}$. Figure 6 represents these interface phenomena.

The discrepancy between the current calculated from Equation 1 (using the Nelder simplex method [15]) and the experimental values eliminate the seven-parameter model (see Figs 7 and 8). Since the most important shift is observed in the passivation range, the model has been modified by decomposing the direct dissolution of monovalent nickel, i.e. $[Ni(I)]_{ads} \rightarrow [Ni(II)]_{sol1}$, in two steps. This new model is shown in Fig. 9.

The current-potential relationship corresponding to this model is:

$$I = \frac{2F(K_2 + K_3)}{1 + K_2\left(\frac{1}{K_1} + \frac{1}{K_5}\right) + K_3\left(\frac{1}{K_1} + \frac{1}{K_4}\right)} \qquad (2)$$

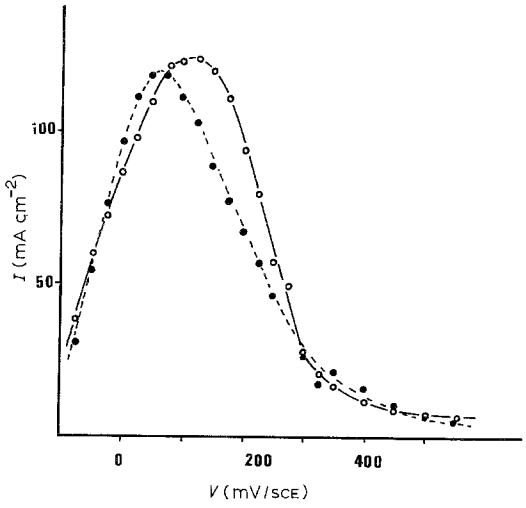

Fig. 7. Comparison between experimental (O) and calculated (●) I–V curves from the seven-parameter model. 270 Ni (recrystallized no. 2); ε = 0.1; K_2SO_4 + LiOH at 23.5° C.

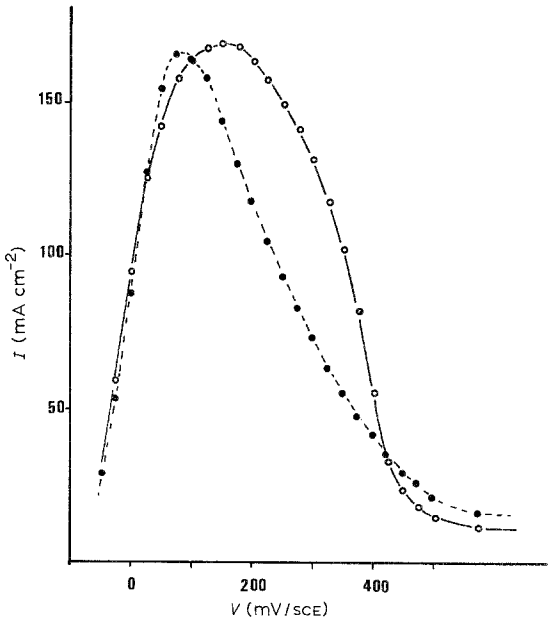

Fig. 8. Comparison between experimental (O) and calculated (●) I–V curves from the seven-parameter model. 270 Ni (recrystallized no. 2); ε = 0.25; K_2SO_4 + LiOH at 23.5° C.

The phenomena taking place at the interface are represented in Fig. 10.

The quasi-identity between the experimental and the calculated profiles, through Equation 2, confirms the present hypotheses and renders the model plausible (see Figs 11 and 12). In order to evaluate the role of cold-hammering on kinetics, the rate constants were recalculated by fitting the experimental curves by Equation 2 in which the values of the Tafel exponents were fixed. The value taken for each Tafel exponent is the mean of the values calculated for the two deformation ratios. Table 4 gives the kinetic parameters obtained.

By comparing the elementary steps associated to deformations ε = 0.1 and ε = 0.25, it is seen (Table 4) that there is a relative decrease in the formation of the Ni(II) species in the passive branch with respect to the active branch when ε increases (K_2^0/K_3^0 is 15 times higher for ε = 0.25 than for ε = 0.1). A significant increase of the chemical dissolution rates (K_4 and K_5) is simultaneously observed, in particular for the stable passivation branch, which leads to a

Table 4. Kinetic parameters as a function of ε ($a = 0.0295\,mV^{-1}$; $b_1 = 0.0139\,mV^{-1}$; $b_2 = 0.0385\,mV^{-1}$)

270 Ni recrystallized no. 2 Kinetic parameters ($mmol\,cm^{-2}\,s^{-1}$)	ε = 0.1	ε = 0.25
K_1^0	0.72×10^{-2}	1.35×10^{-2}
K_2^0	1.58×10^{-3}	1.7×10^{6}
K_3^0	0.28×10^{-6}	0.2×10^{2}
K_5	0.72×10^{-3}	0.88×10^{-3}
K_4	0.4×10^{-4}	0.64×10^{-4}
K_2^0/K_3^0	5.64×10^{3}	8.5×10^{4}
K_5/K_4	1.8	1.38

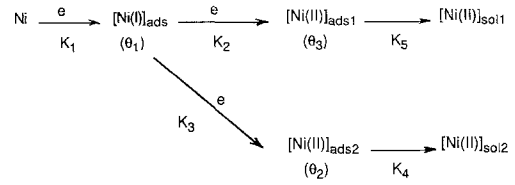

Fig. 9. Model for the dissolution-passivation of Ni in neutral and alkaline media (eight kinetic parameters).

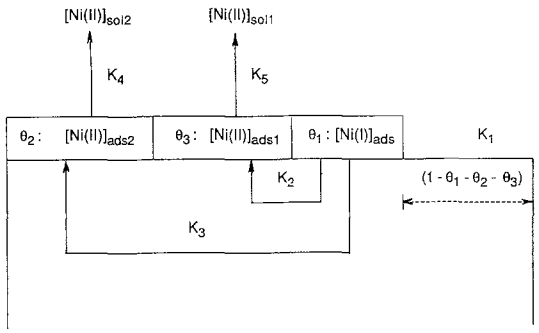

Fig. 10. Schematic representation of interface phenomena between the metal substrate and the electrolyte for a unit surface: θ_1, θ_2 and θ_3 represent the coverage fractions of the reaction intermediates.

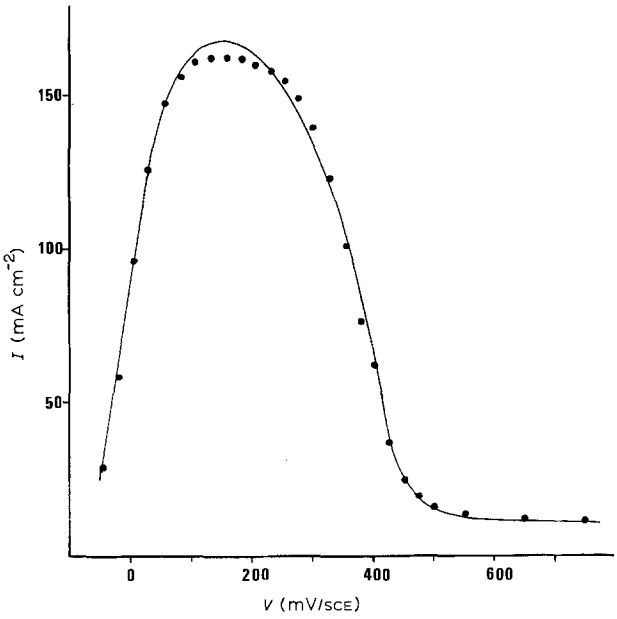

Fig. 12. Comparison between experimental (O) and calculated (●) I–V curves from the eight-parameter model. 270 Ni (recrystallized no. 2); $\varepsilon = 0.25$; K_2SO_4 + LiOH at 23.5° C.

decrease in the K_4/K_5 ratio (1.3 times lower). The $Ni(OH)_2$ or NiO is more rapidly destroyed than formed when ε increases.

Since the ε increase is associated with a higher sulphur concentration at the interface, it may be assumed that sulphur is a depassivating factor: it prevents the adsorption of OH^- ions or H_2O molecules [9] which are required to form the passivating species. Confirmation of the significance of corrosion in the presence of sulphur is provided by both the morphology and the topography of the corrosion states shown in Fig. 4. In addition, the relatively homogeneous distribution of the corrosion products, independently of the polishing grooves, shows that the initial mechanical polishing has no influence on the corrosion morphology.

Since no steady-state can be obtained in H_2SO_4, the

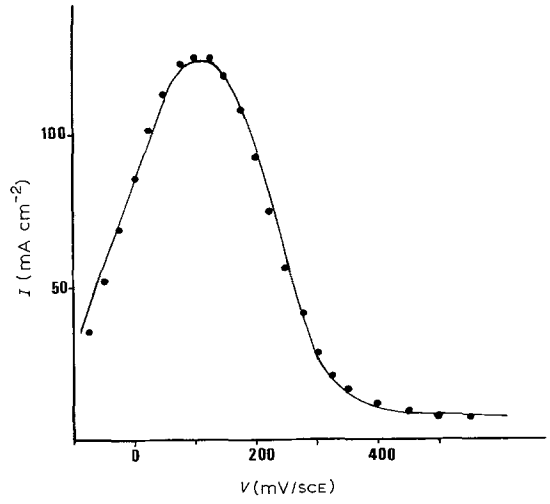

Fig. 11. Comparison between experimental (O) and calculated (●) I–V curves from the eight-parameter model. 270 Ni (recrystallized no. 2); $\varepsilon = 0.1$; K_2SO_4 + LiOH at 23.5° C.

I–V curves cannot be parametered accurately. However, the model proposed for the alkaline medium is still appropriate considering the shape of the experimental plots. The marked medium acidity accelerates the dissolution branch and decelerates the passivation branch. The partial reaction orders, with respect to OH^-, which intervene at the level of the various steps, make the depassivating effect of sulphur relatively less marked in neutral than in alkaline medium (see Table 5 for the ratio between currents).

It should be noted that the present approach does not take account of localized corrosion, mainly at the level of pits where the dissolution rate is necessarily higher. Localized corrosion may be taken into account by a further model in which two types of sites exist at the initial interface. The same reaction mechanism as that proposed here would take place at these sites, but with different rates. These sites would correspond to two different surface concentrations of sulphur. Confirmation of such a hypothesis requires a quantitative knowledge of the initial spatial distribution of sulphur, which is difficult owing to the magnitude of the sulphur concentration (one or less than one monolayer, on average). The discrepancy between the experimental and calculated curves may be indicative of the existence of the two types of sites prior to dissolution.

Table 5. Quantities characterizing the current as a function of the medium, from potentiodynamic plots

Reference Ni / *Recrystallized Ni*	*H_2SO_4 (1 M)*	*K_2SO_4 + LiOH pH ~ 9.5*
Maximum current	12.6	37.1
Passivity current	3.8	11.2

5. Conclusion

The effect of sulphur segregation on the surface of 270 nickel has been revealed through analysis of the *I–V* curves. Sulphur segregation was shown to increase the dissolution rate with respect to the reference metal. This increase is less significant in the K_2SO_4 + LiOH medium, but with a strong intergranular corrosion in acidic medium. The steady-state polarization curves obtained in the alkaline medium can be accounted for by a nickel dissolution model involving a single bifurcation. The corresponding kinetic parameters have been calculated by fitting the experimental curves. By comparing two segregation states obtained from a mechanism out of thermodynamic equilibrium, the dominating roles of sulphur and OH^- ions have been demonstrated. In particular, sulphur is shown to be a blocking element in nickel passivation.

References

[1] A. Larère, M. Guttman, P. Dumoulin and C. Roques-Carmes, *Acta Met.* **30** (1982), 685.
[2] P. Pascal, 'Nouveau Traité de Chimie Minérale', Tome XVII, 2ème fascicule, Masson, Paris (1963) p. 664.
[3] J. Oudar and P. Marcus, *Mem. Sc. Rev. Met.* (1987) 131.
[4] G. Saindrenan and A. Larère, *Scripta Metallurgica* **18** (1984) 969.
[5] G. Saindrenan, D. Roptin, J. M. Maufras and B. Bauche, *ibid.* **23** (1989) 1163.
[6] A. Larère and G. Saindrenan, *J. Physique, Série C*, to be published.
[7] P. Marcus, Thèse d'Etat, Paris VI (1979).
[8] J. P. Frayret, A. Caprani, F. Delrey, A. Moreau and R. Pointeau, *J. Chim. Phys.* **78** (1981) 233.
[9] M. R. Barbosa, S. G. Real, J. R. Vilche and A. J. Ariva, *J. Electrochem. Soc.* **135** (1988) 1077.
[10] A. Jouanneau, Thèse d'Etat, Bordeaux, Numéro d'ordre 439 (1975).
[11] A. Caprani, *J. Chim. Phys.* **2** (1975) 171.
[12] A. Caprani and J. P. Frayret, *Electrochim. Acta* **24** (1979) 835.
[13] J. P. Frayret, A. Caprani and R. Pointeau, *ibid.* **26** (1981) 1789.
[14] A. Caprani and J. P. Frayret, *J. Less Common Metals* **69** (1980) 29.
[15] J. P. Badiali, H. Cachet, A. Cyrot and J. C. Lestrade, *J. Chem. Soc. Faraday Trans. II* **69** (1973) 1339.